Supporting Information For

Self-Enhancement of CO Reversible Absorption Accompanied by Phase Transition in Protic Chlorocuprate Ionic Liquids for Effective CO Separation from N_2

*Zhuo-Heng Tu, Yi-Yang Zhang, You-Ting Wu*and Xing-Bang Hu **

School of Chemistry and Chemical Engineering, Separation Engineering Research Centre, Key Laboratory of Mesoscopic Chemistry of MOE, Nanjing University, Nanjing 210093 (P. R. China). E-mail: ytwu@nju.edu.cn (Y. Wu); huxb@nju.edu.cn (X. Hu)

Index

1. Materials

2. Synthesis of [TEA][$CuCl_2$]

3. Characterization of PCILs

4. Stability of [TEA][$CuCl_2$] in the air

5. CO absorption experiments

6. Evidence for phase change in [TEA][$CuCl_2$] during CO absorbtion

7. CO desorption/releasing experiments

8. Regeneration process of the PCILs

9. Membrane preparation and gas permeation measurement

10. Theoretical calculations

11. Equilibrium thermodynamic properties of CO absorption in PCILs

1. Materials. CO (99.9%) and N_2 (99.9%) was supplied from Nanjing Special Gas Co.Ltd.; Trimethylamine hydrochloride(CP grade, 99%), Triethylamine(CP grade, 99%) and tripropylamine(CP grade, 99%) were purchased from Sinopharm Chemical Reagent Co.Ltd.; Cuprous chloride(AR grade, 97%) was obtained from aladdin Industrial Co.Ltd.; The other regular reagents and solvents were purchased from Shanghai Lingfeng Chemical Reagent Co.Ltd. The porous membrane support used in this work was hydrophilic polyethersulfone (PES) flat sheet membrane with a pore size of 0.2 μm, porosity of 80%, average thickness of 119 μm and effective area of 64 cm^2, which was purchased from Beijing Membrane Corporation. Cuprous chloride was purified through the recrystallization in HCl aqueous solution and the final drying. Other reagents were used without further purification.

2. Synthesis of [TEA][$CuCl_2$]. A two-step synthetic procedure was uesd to prepare the protic chlorocuprate ionic liquids (PCILs): the first step is the synthesis of tertiary ammonium hydrochloride by neutralization reaction. For example, 8.33 ml (0.1 mol HCl) hydrochloric acid (37%) was slowly added into 10.12 g (0.1 mol) triethylamine (TEA) which was loaded into a 250 ml flask in advance. The flask was placed in cold water bath and the mixture in the flask was vigorously stirred with a magnetic stirrer for 1 h. The resulting solution was then distilled using a rotary evaporator to remove a large proportion of water. The residue was washed with 10 ml diethyl ether for three times and dried in vaccum oven at 0.1 kpa and 60 °C for at least 3 days. 13.65 g (yield > 99%) white solid powder was obtained for further grinding. The second step was the mixing of 6.88 g (0.05 mol) triethylamine hydrochloride with 4.95 g (0.05 mol) purified CuCl in a sealed flask with vacuum valve under N_2 protection. The mixture in the flask was heated and stirred under 60 °C for 4 h. A chartreuse liquid

product was finally obtained with a yield of 100%. The same preparation methodology was followed for the synthesis of trimethylamine (TMA) chlorocuprate and tripropylamine (TPA) chlorocuprate. The mass fraction of water in the samples were measured using Karl- Fisher Coulometric Titration (Brinkmann Metrohm 787 KF Titrino) to be less than 0.05% for all the dried samples.

3. Characterization of PCILs. The structure of PCILs was confirmed with the ^{1}H and ^{13}C NMR spectra (BRUKER AV 400 MHz), Attenuated Total Reflectance Infrared (ATR-IR) Spectroscopy (NICOLET iS10) and elemental analysis (Heraeus CHN-O-Rapid). The determination of physico-chemical parameters was performed on analytical instruments such as Densimeter (DMA 5000 density meter), Viscometer (HAAKE Rheostress 600), Thermogravimetric Analysis (Perkin-Elmer TG/DTA, 2010) and Different Scanning Calorimetry (Perkin-Elmer Diamond DSC). The glass transition temperature (T_g) and melting temperature (T_m) were recorded in the temperature range of -100 to 0 °C and 20 to 600 °C under N_2 atmosphere, at a scan rate of 10 °C/min. The temperatures of decomposition (T_{dec}) were recorded at a scan rate of 10 °C/min under N_2 atmosphere and in the temperature range of 20 to 500 °C.

[TMA][$CuCl_2$]: ^{1}H NMR (400 MHz, CD_3CN) δ = 2.82 (s, 9H). ^{13}C NMR (101 MHz, CD_3CN) δ = 44.65 (s). IR: 3114, 3026, 2754, 2513, 2468, 1474, 1459, 1409, 1250, 1050, 976, 816, 560 cm^{-1}. CHN elemental analysis (%), calculated: C 18.50, H 5.14, N 7.20, found: C 18.35, H 5.34, N 7.17.

[TEA][$CuCl_2$]: ^{1}H NMR (400 MHz, DMSO) δ = 8.84 (s, 1H), 3.10 (q, J=7.3, 6H), 1.18 (t, J=7.3, 9H). ^{13}C NMR (101 MHz, DMSO) δ = 46.33 (s), 9.24 (s). IR: 2980, 2784, 2688,

2489, 1460, 1392, 1359, 1290, 1173, 1158, 1060, 1031, 1013, 836, 807, 792, 737, 555, 538, 463 cm^{-1}. CHN elemental analysis (%), calculated: C 30.45, H 6.76, N 5.92, found: C 30.32, H 6.84, N 5.87.

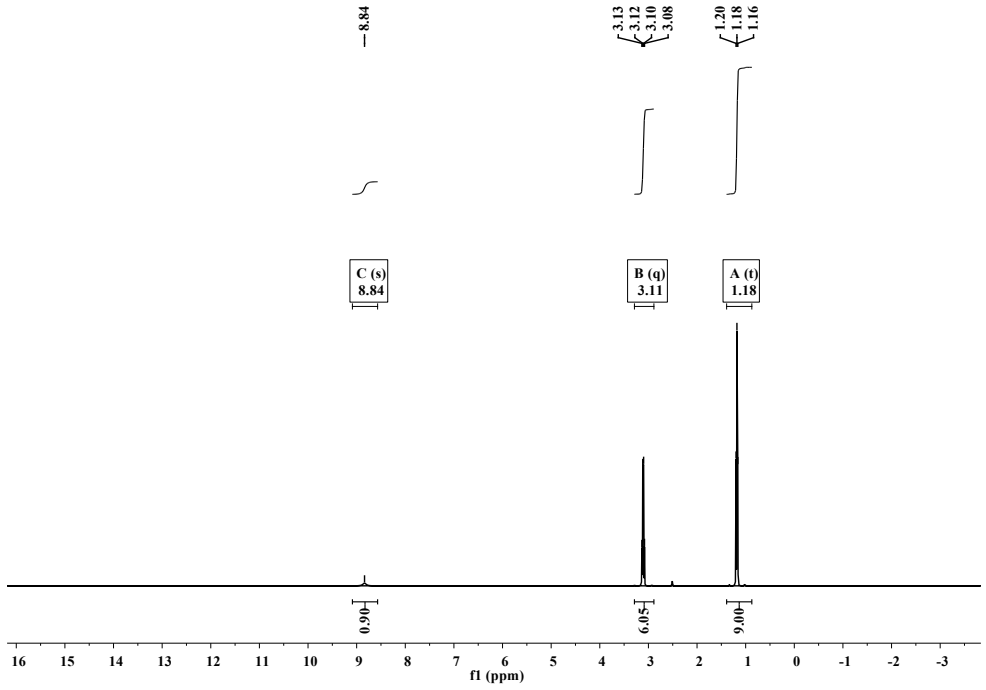

Figure S1 ^{1}H-NMR spectrum of [TEA][$CuCl_2$] in DMSO-d_6.

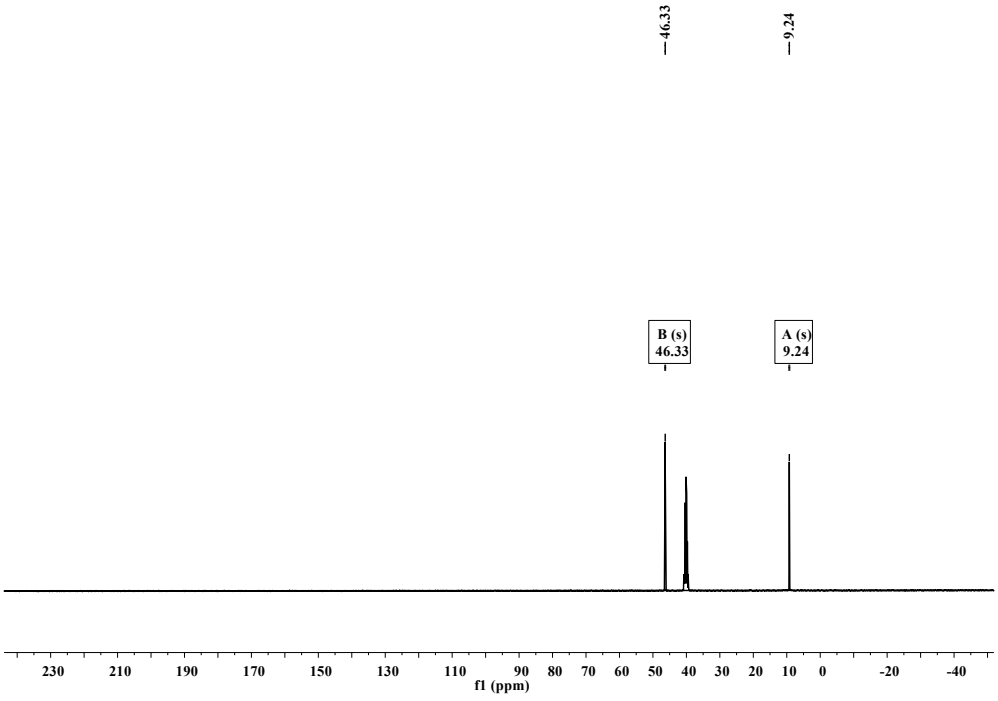

Figure S2 ^{13}C-NMR spectrum of [TEA][$CuCl_2$] in DMSO-d_6.

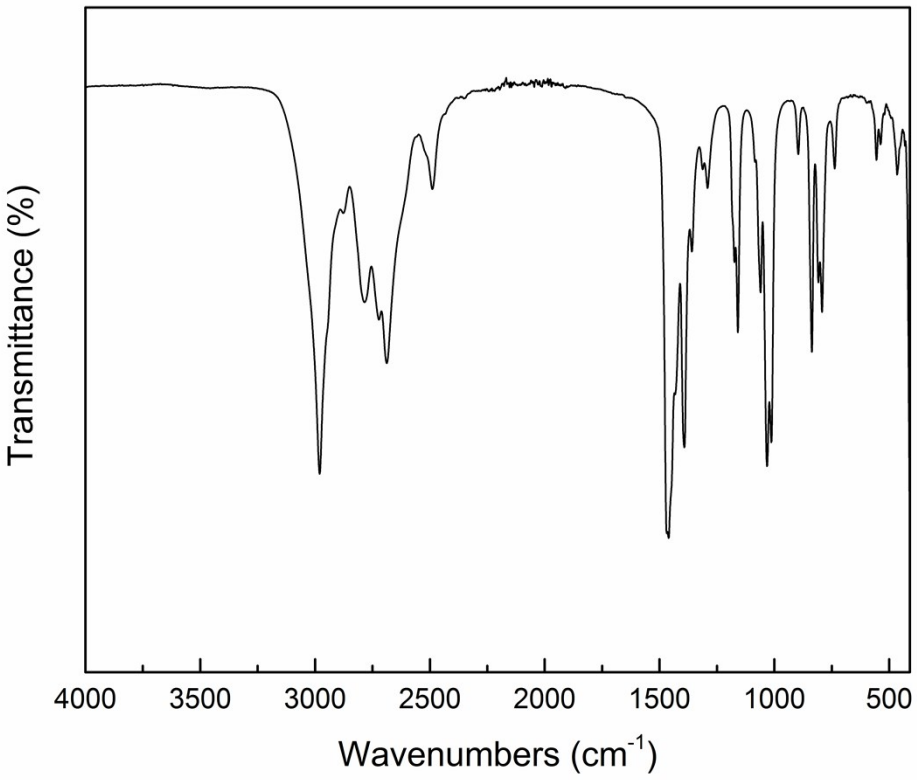

Figure S3 FTIR spectrum of [TEA][$CuCl_2$].

[TPA][$CuCl_2$]: ^{1}H NMR (400 MHz, DMSO) δ = 8.87 (s, 1H), 3.02 – 2.99 (t, 6H), 1.68 – 1.58 (m, 6H), 0.91 (t, J=7.4, 9H). ^{13}C NMR (101 MHz, DMSO) δ = 54.13 (s), 17.24 (s), 11.35 (s). IR: 2967, 2878, 2777, 2661, 2527, 1470, 1381, 1092, 1043, 984, 753 cm^{-1}. CHN elemental analysis (%), calculated: C 38.78, H 7.89, N 5.02, found: C 38.72, H 7.92, N 5.02.

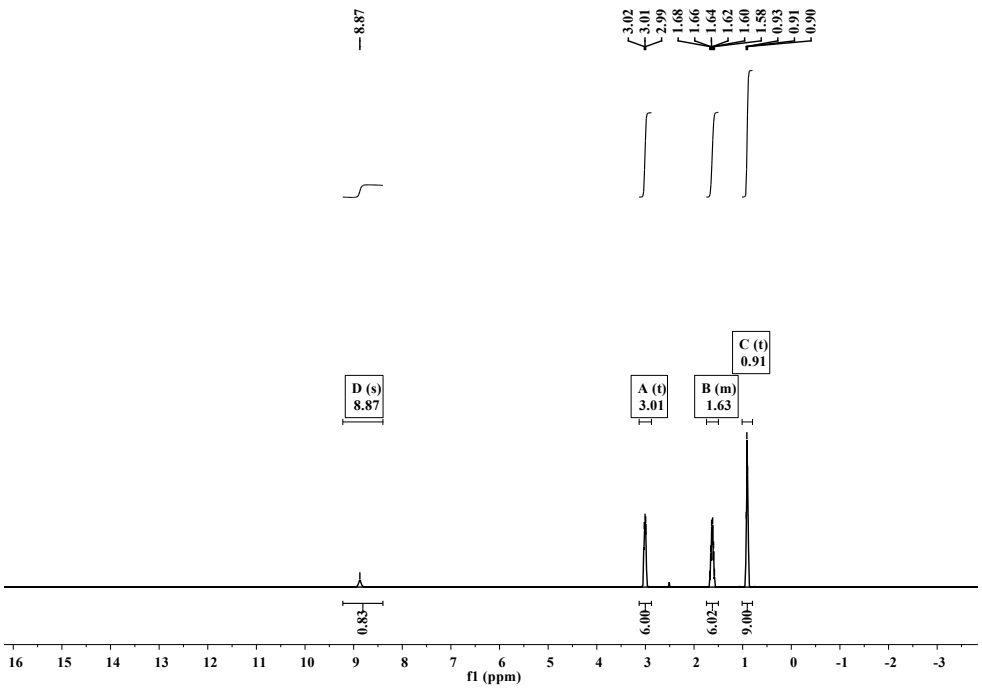

Figure S4 ^{1}H-NMR spectrum of [TPA][$CuCl_2$] in DMSO-d_6.

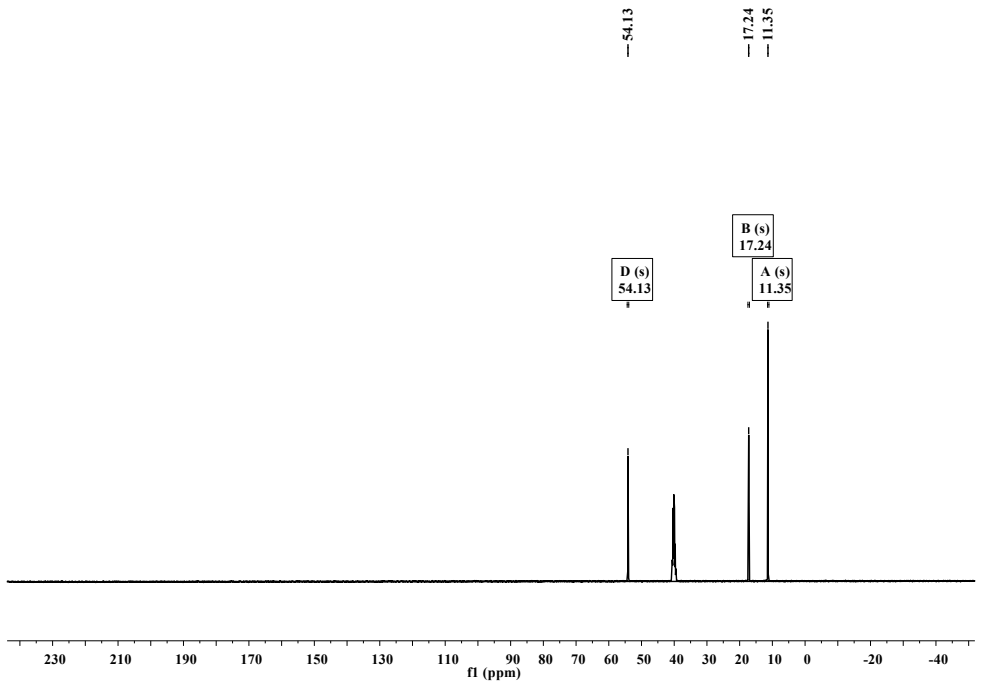

Figure S5 ^{13}C-NMR spectrum of [TPA][$CuCl_2$] in DMSO-d_6.

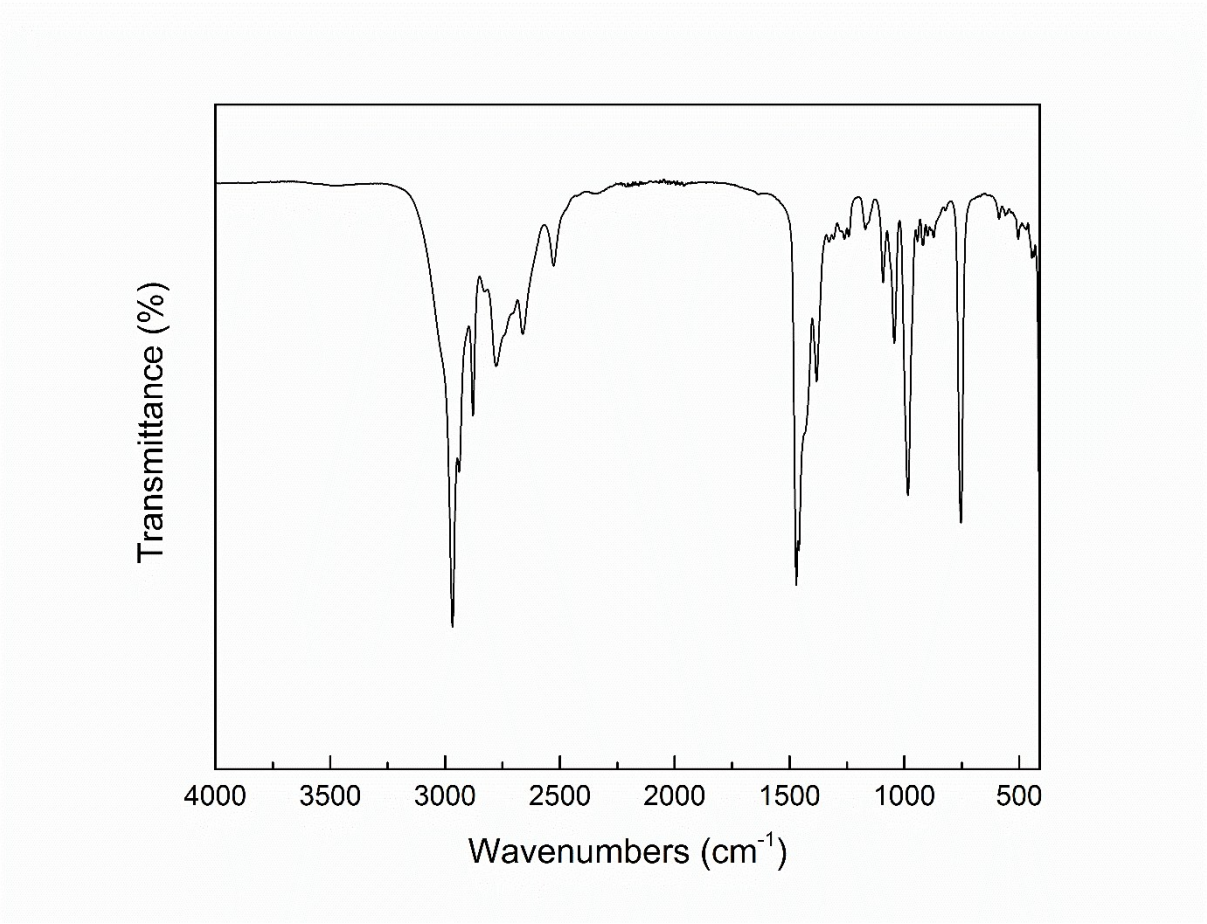

Figure S6 FTIR spectrum of [TPA][$CuCl_2$].

Table S1 Physico-chemical properties of PCILs.

PCILs	T_g/°C	T_m/°C	T_d/°C	M/g·mol^{-1}	ρ/g·cm^{-3}	η/cP
[TMA][$CuCl_2$]	ND[a]	112	245	194.57	ND[a]	NA[a]
[TEA][$CuCl_2$]	-73	ND[a]	229	236.65	1.4319[b]	77.9[b]
[TPA][$CuCl_2$]	-62	ND[a]	232	278.73	1.2602[b]	214.1[b]

[a]ND: not detected. NA: not available.

[b]properties measured at 30 ºC

Table S2 Densities and Viscosities of PCILs at various temperatures.

PCILs	T(K)	Density (g/cm^3)	Viscosity (cP)
[TEA][$CuCl_2$]	298.15	1.4388	103.4
	303.15	1.4342	77.9
	313.15	1.4250	53.3
	323.15	1.4161	38.1
	333.15	1.4072	24.1
[TPA][$CuCl_2$]	298.15	1.2643	339.2
	303.15	1.2602	214.1
	313.15	1.2518	107.3
	323.15	1.2439	62.2
	333.15	1.2360	40.1

4. Stability of [TEA][$CuCl_2$] in the air. To test the stability of [TEA][$CuCl_2$] in the air, FT-IR was used to detect the structural change of [TEA][$CuCl_2$] exposed in the air at different times (Figure S7). It is worth noting that within half an hour, there is no obvious change in the range of 3000 to 3500 cm^{-1}, which means that [TEA][$CuCl_2$] are stable in the air in a short time. But a wide peak around 3300 to 3600cm^{-1} appeared in FTIR spectrum of [TEA][$CuCl_2$] after exposed in the air for 1 hour, which corresponds to the water absorbed in [TEA][$CuCl_2$]. Two peaks appeared at 3355 and 3454 cm^{-1} after 4 hours, which may be due to stretching vibration of (HO-Cu-)OH and (Cl-Cu-)OH in the generated $Cu_2(OH)_3Cl$, which is consistent with that reported in literature.[1,2] This means that long time exposure of these ILs in the air will lead to structure change of ILs. Therefore, in order to avoid the side effects of oxygen and moisture on the experimental results, most experiments are operated under the protection of nitrogen in this work to avoid long-term contact with air.

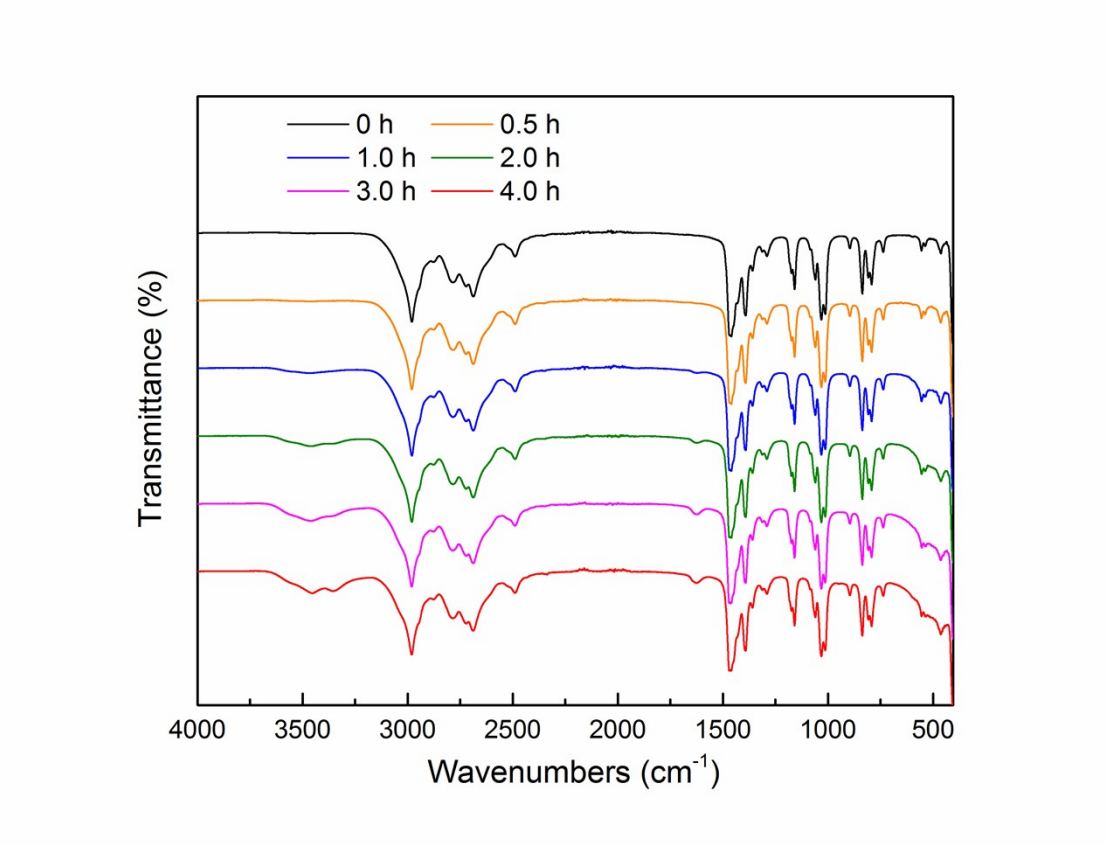

Figure S7. FT-IR spectra of [TEA][$CuCl_2$] exposed in the air at different times (relative humidity: 30%, room temperature: 15 ºC).

5. CO absorption experiments. Apparatus for the determination of CO absorption in these PCILs is similar to our group's previous report on SO_2 absorption determination.[3] The whole device consists of two 316 L stainless steel chambers whose volumes are 117.581 cm^3 (V_1) and 84.460 cm^3 (V_2), respectively. The bigger chamber, named as gas reservior, isolates and stores CO before it contacts with the absorbents in the smaller chamber. The smaller chamber used as equilibrium cell is equipped with a matched beaker and a magnetic stirrer. The temperatures (T) of both chambers are controlled by a water bath with an uncertainty of ± 0.1 K. The pressures in the two chambers are monitored using two pressure transducers (Wideplus Precision Instruments Co., Ltd.) of ± 0.2% uncertainty (in relation to the full scale).

The pressure transducers are connected to a Numeric Instrument (WP-D821-200-1212-N-2P) to record the pressure changes online. In a typical run, a known mass (w) of a PCIL absorbent is placed into the equilibrium cell and the air in the two chambers is evacuated (<10 Pa). The pressure in the equilibrium cell is recorded to be P_o. CO from a gas cylinder is then fed into the gas reservior to a pressure of P_1. The needle valve between the two chambers is turned on to let CO be introduced to the equilibrium cell. Absorption equilibrium is thought to be reached when the pressures of the two chambers remained constant for at least 1 h. The equilibrium pressures are denoted as P_2 for the equilibrium cell and P'_1 for the gas reservior. The CO partial pressure in the equilibrium cell is $P_S = P_2 - P_o$. The CO uptake, $n(P_S)$, can thus be calculated using the following equation:

$$n(P_S) = \rho_g(P_1, T)V_1 - \rho_g(P'_1, T)V_1 - \rho_g(P_S, T)(V_2 - w/\rho_{IL}) \quad (S1)$$

where $\rho_g(P_i, T)$ represents the density of CO in mol/cm^3 at P_i (i =1,S) and T, and is calculated according to the NIST Standard Reference Database. ρ_{IL} is the density of the PCILs in g/cm^3 at T. V_1 and V_2 represent the volumes in cm^3 of the two chambers, respectively. Continual determinations of solubility data at elevated pressures are performed by introducing more CO into the equilibrium cell to reach new equilibrium. The solubility of CO is defined as the molar ratio of CO to IL in this work. Duplicate experiments were run for each PCIL to obtain averaged values of CO absorption. The averaged uncertainty of the absorption data in this work was well within ± 1%. The same procedure was followed for the determination of N_2 absorption in PCILs, and the data were shown in Figure 1 of the manuscript.

A supplementary explanation of Figure 1 is presented here. The curve increases slowly from c to d, and there is a slight change from c to d in CO absorption efficiency (0.072 mol_{CO}/mol_{IL}) in Figure 1 after the appearance of solid at point c. This is because the solid

produced in the upper layer of the IL will hinder direct contact of the IL with CO gas (see Figure S10). When the CO pressure exceeds 6 bar (point d to e), the remaining IL transforms into solid slowly due to the slow mass transfer rate. This is why liquid-solid to solid transition was not abrupt.

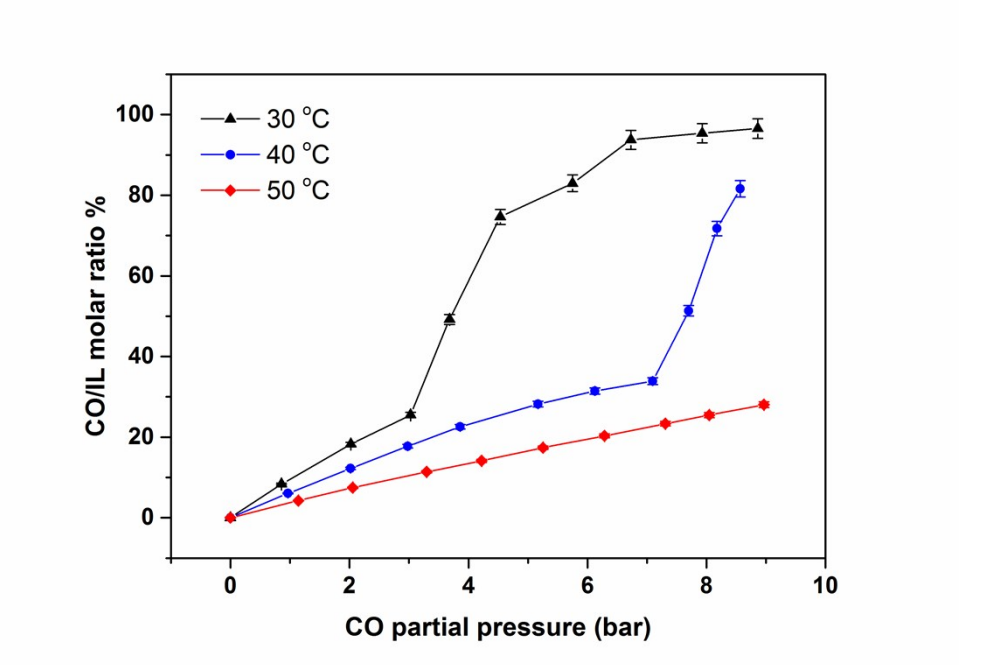

Figure S8 Solubility of CO in [TPA][$CuCl_2$] under different CO pressures and temperatures.

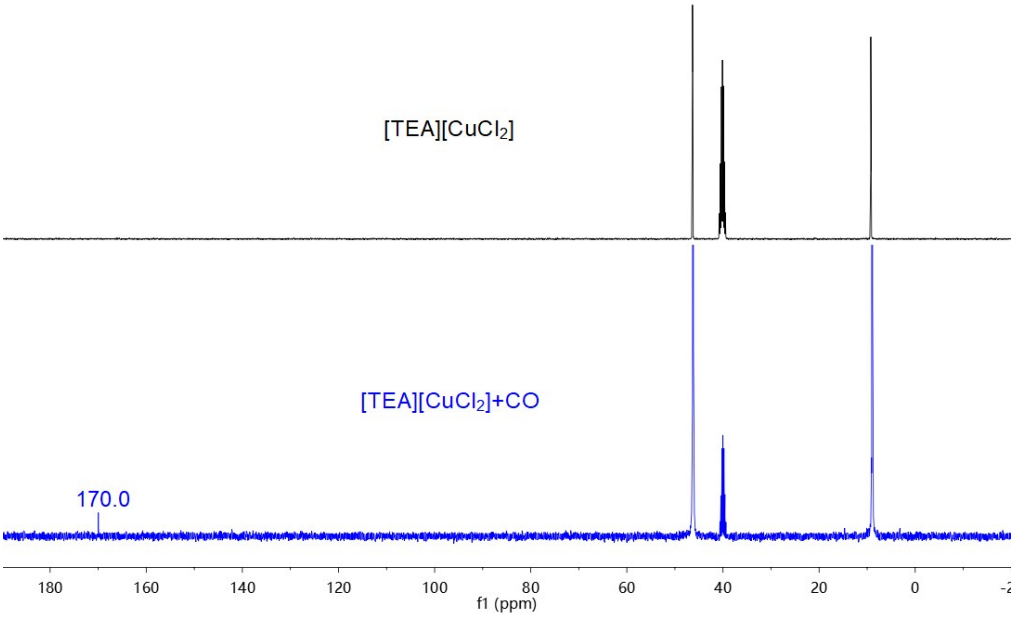

Figure S9 ^{13}C NMR spectra of [TEA][$CuCl_2$] before and after the capture of CO.

Table S3 A summary of the solubility of CO and N_2 and the selectivity of CO/N_2 in [TEA][$CuCl_2$].

Gas	Temperature (°C)	$R_{0.1}$[a] (mmol/mol)	$R_{0.9}$[b] (mmol/mol)	$R_{4.0}$[c] (mmol/mol)	$R_{7.0}$[d] (mmol/mol)	$S_{0.1/0.1}$[e]	$S_{0.9/0.9}$[f]	$S_{4.0/4.0}$[g]	$S_{7.0/7.0}$[h]	$F_{0.1/0.9}$[i]
CO	30	8.252 ±0.190	68.26 ±1.84	591.9 ±12.4	822.5 ±24.7	102.2 ±4.6	94.1 ±5.3	176.3 ±7.2	134.2 ±7.1	102.4 ±5.3
N_2	30	0.08072 ±0.00177	0.7255 ±0.0210	3.358 ±0.067	6.130 ±0.141					
CO	40	4.585 ±0.115	48.17 ±1.25	175.3 ±4.9	272.7 ±5.7	70.3 ±3.2	82.2 ±4.1	65.8 ±3.8	54.9 ±2.6	70.4 ±3.4
N_2	40	0.06516 ±0.00130	0.5863 ±0.0141	2.662 ±0.077	4.968 ±0.134					

[a] Solubility at 0.1 bar

[b] Solubility at 0.9 bar

[c] Solubility at 4.0 bar

[d] Solubility at 7.0 bar

[e] Selectivity defined as $R_{CO,0.1}/R_{N2,0.1}$

[f] Selectivity defined as $R_{CO,0.9}/R_{N2,0.9}$

[g] Selectivity defined as $R_{CO,4.0}/R_{N2,4.0}$

[h] Selectivity defined as $R_{CO,7.0}/R_{N2,7.0}$

[i] Separation factor defined as $(R_{CO,0.1}/R_{N2,0.9})/(0.1/0.9)$

6. Evidence for phase change in [TEA][$CuCl_2$] during CO absorption. About 2.0 g PCIL and a magnetic stirrer were put into a glass bottle in stainless steel chamber under different CO pressure and room temperature for 12 h to get the CO-saturated absorbent. A needle was pierced through the cap to prevent contact with air and high pressure inside the bottle when the glass bottle was taken out from stainless steel chamber. The photos of fresh [TEA][$CuCl_2$] and CO-saturated [TEA][$CuCl_2$] were taken with the aid of a laser pointer and are shown in Figure S10. The fresh [TEA][$CuCl_2$] was clear and transparent, and the laser could pass through the IL to form a bright and concentrated spot on the whiteboard behind the glass bottle (Figure S10a and S10b). After absorbing CO at 5 bar, there was obvious solid generated in the upper layer of the IL, and the laser light in the IL became divergent and the spot on the whiteboard turned bigger and weaker. This is because the solid particles generated

in the ionic liquid scattered the laser light (Figure S10c). After absorbing CO at 9 bar, the IL completely turned into solid ,and there was no spot generated on the whiteboard, indicating that the laser light could not pass through the glass bottle anymore (Figure S10d and Figure S10e).

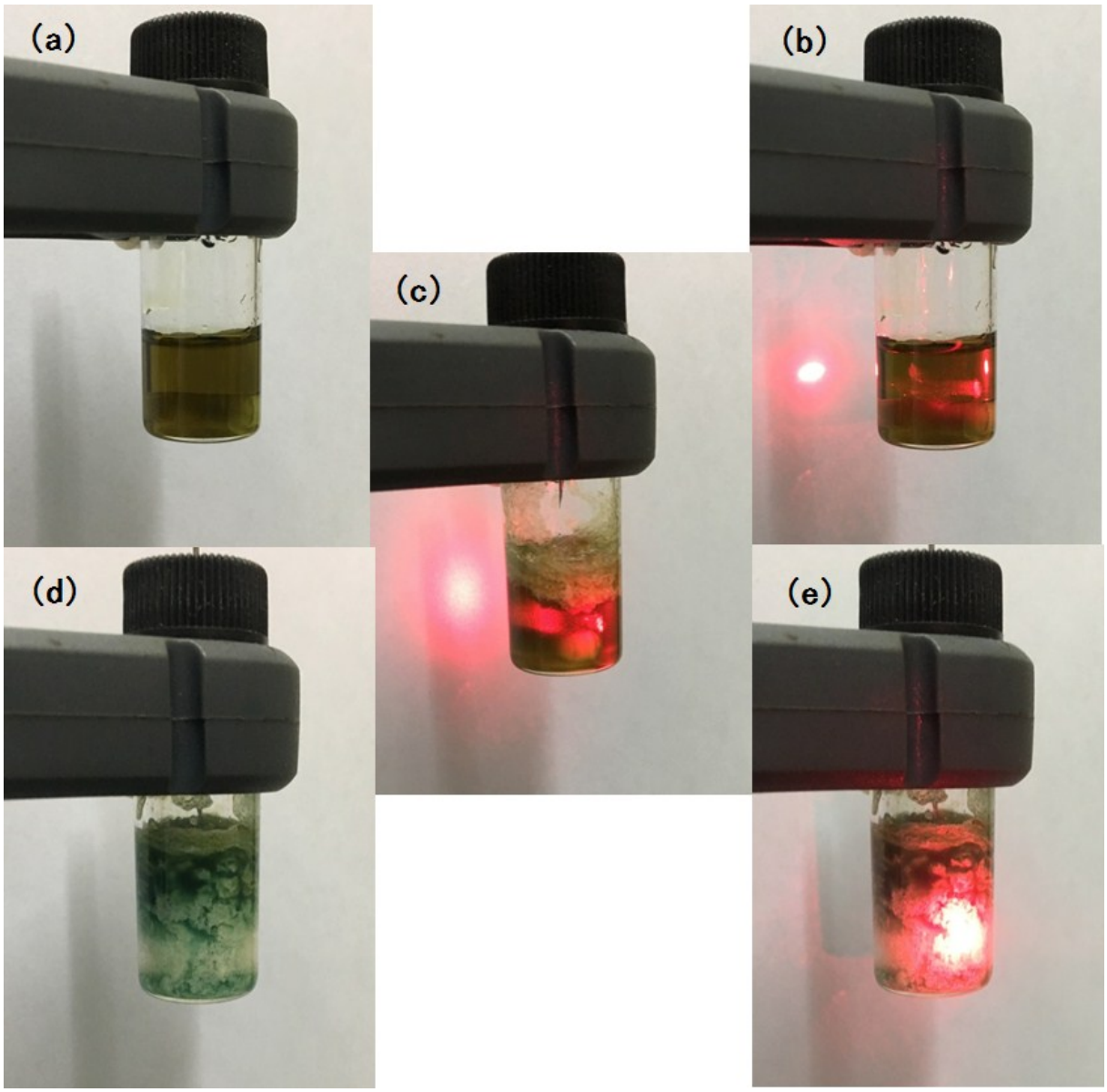

Figure S10 Photos of (a) fresh [TEA][$CuCl_2$]; (b) fresh [TEA][$CuCl_2$] under the illumination of the laser; (c) [TEA][$CuCl_2$] saturated with CO (5 bar) under the illumination of the laser; (d) [TEA][$CuCl_2$] saturated with CO (9 bar); (e) [TEA][$CuCl_2$] saturated with CO (9 bar) under the illumination of the laser.

7. CO desorption/releasing experiments. About 2.0 g PCIL was put into the high pressure reactor under 3 Mpa CO pressure and room temperature for 12 h to get the CO-saturated absorbent. The absorbed amount of CO was determined from the mass difference of the initial PCIL and the CO-saturated absorbent using a balance (±0.0001g). The CO release efficiency was investigated using the following physical and chemical methods.

a) The absorbents were handled under still-setting or 500 rpm magnetic stirring at room temperature. N_2 atmosphere was used to prevent the trouble of oxidation and hydrolysis. The released amount of CO gas was determined from the mass change.

b) The absorbed CO in the absorbents was released under 500 rpm magnetic stirring and heating at different temperatures. The released gas volume was measured using a U tube drainage gas gathering equipment.

c) The absorbents were heated using microwave generator at different powers. The released amount of CO gas was determined from the mass change.

d) The absorbents were put into 20 ml solvents. The released amount of CO gas was determined from the mass change.

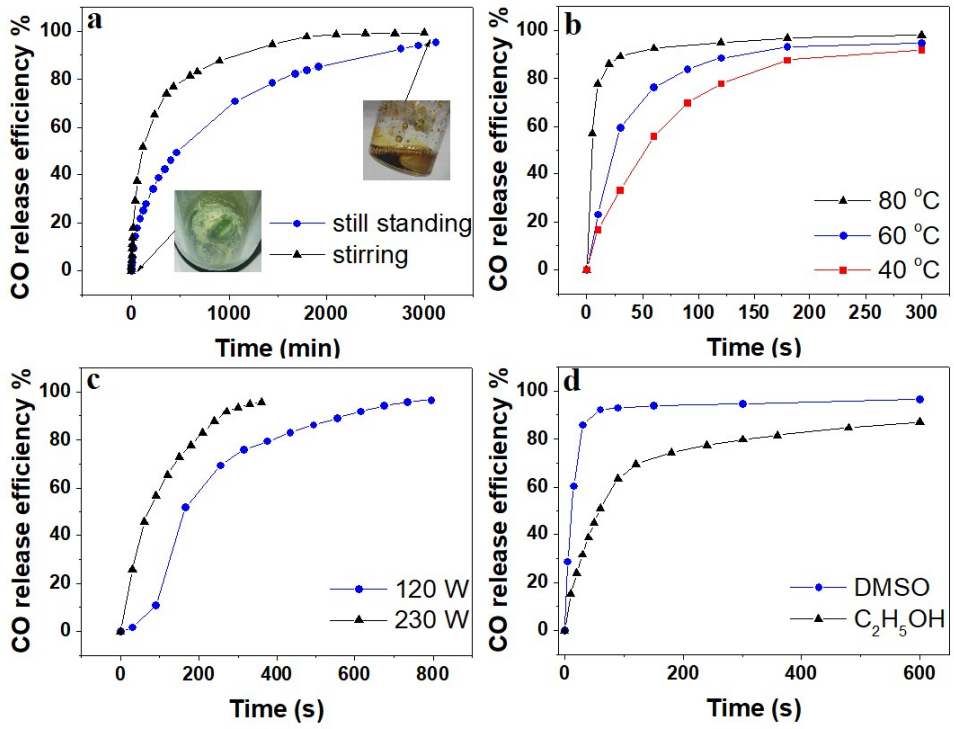

Figure S11 CO release efficiency under (a) still-setting or stirring at room temperature, (b) heating and stirring at different temperatures, (c) microwave and (d) solvents.

8. Regeneration process of the PCILs. The dual-chamber apparatus mentioned above was used to determine the absorption capacity of the PCILs, as well as the reversibility of the absorption. In a typical run, 2.0 g PCIL was added into the equilibrium cell, and CO was absorbed at 30 ºC and 8 bar for 24 h. At the end of each absorption, the consecutive desorption experiment was followed by heating the sample to 80 °C and reducing the pressure to 0.1 kPa in 1 h.

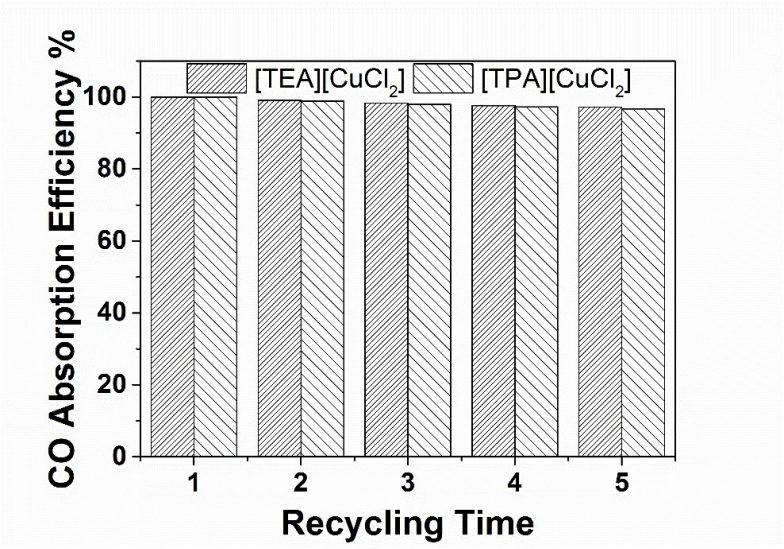

Figure S12 Recycle of [TEA][$CuCl_2$] and [TPA][$CuCl_2$] for CO absorption.

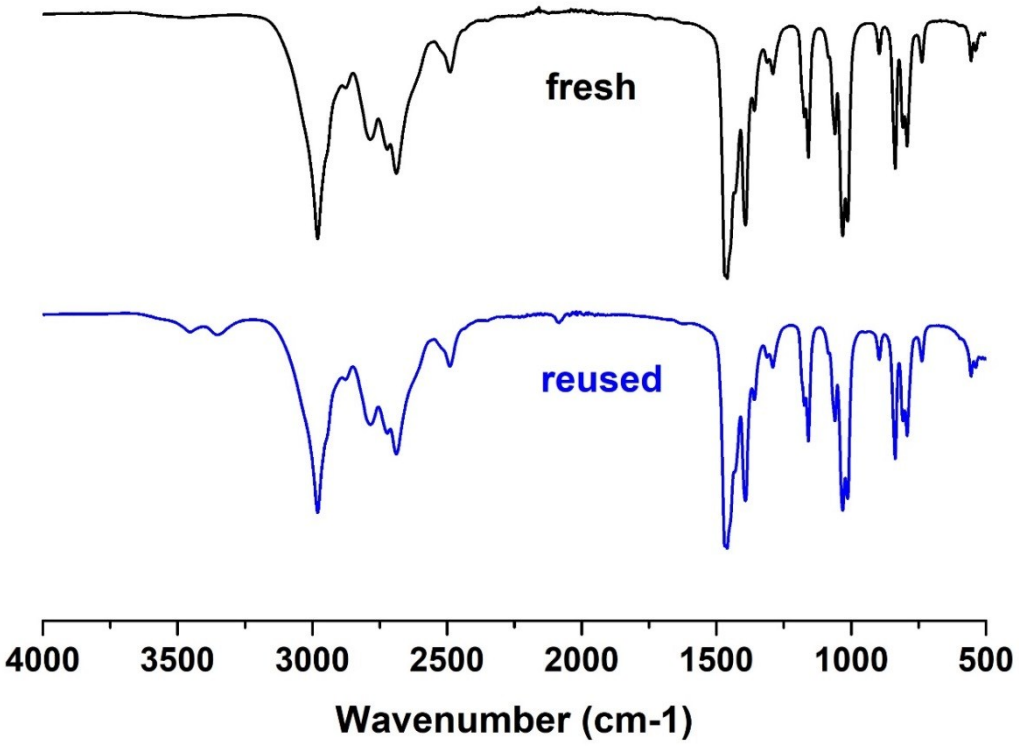

Figure S13 FTIR spectra of the fresh and reused [TEA][$CuCl_2$].

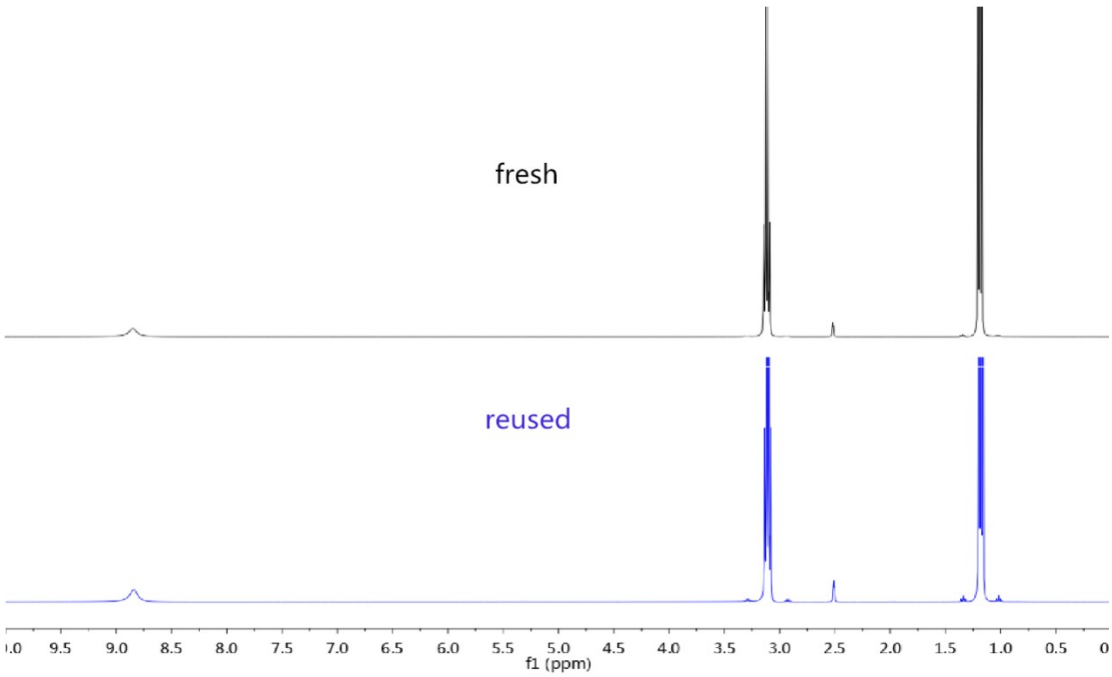

Figure S14 ^{1}H NMR spectra of the fresh and reused [TEA][$CuCl_2$]

9. Membrane preparation and gas permeation measurement. Hydrophilic polyethersulfone (PES) flat sheet membrane was chosen as porous membrane support. The preparation of supported ionic liquid membranes (SILMs) were performed using the impregnation method we used before.[4-6] Firstly, PES membrane was soaked in [TEA][$CuCl_2$] for 12 h for the introduction of PILs into its porous structure. After that, excess ionic liquid was wiped away carefully from the membrane surface with a filter paper and then installed into the test unit. All the above operations are under the protection of nitrogen atmosphere.

The detailed description of the gas permeation measurement apparatus and the experimental procedure is available in our previous work.[5, 7, 8] The single gas permeability of N_2, CH_4, and CO is determined using Eq. (S1) and (S2)

$$P = \frac{L}{\Delta p}\frac{V}{ART}\frac{dp_2}{dt} \quad \text{(S1)}$$

$$\Delta p = p_1 - p_2 \tag{S2}$$

where P is the permeability coefficient, V is the volume of the downstream chamber (cm^3) of the cell, L is the thickness of the membrane (cm), A refers to the effective area of the membrane (cm^2), R is the gas constant, T is the absolute temperature (K), p_1 is the upstream pressure, p_2 is the downstream pressure, and $\frac{dp_2}{dt}$ is the rate of gas pressure increase on the permeate side.

The permeability data of CO and N_2 were measured under 0.1 to 1.5 bar transmembrane pressure difference and 40 ºC. All measurements were done in triplicate and average values were presented in Figure S15 and Table S4.

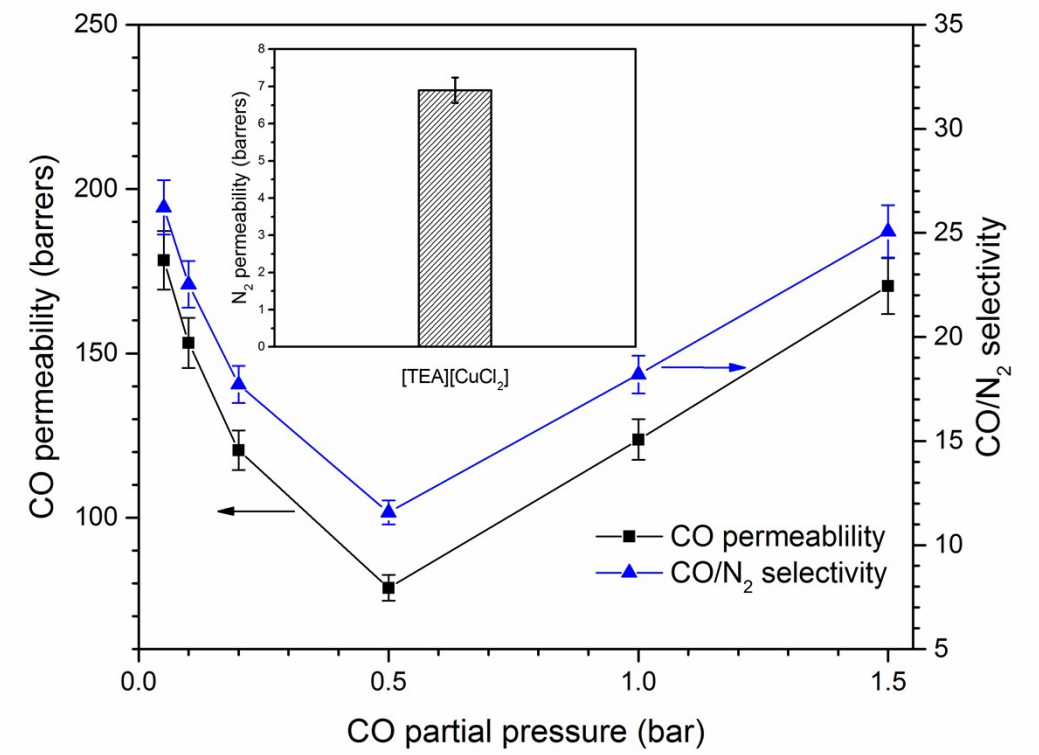

Figure S15 Plots of permeability of N_2 (ΔP=1 bar), CO and ideal selectivity of CO/N_2 in [TEA][$CuCl_2$] based SILMs as a function of transmembrane pressure at 40 ºC.

Table S4 Comparison of CO permeability and CO/N_2 selectivity in reported membranes.

Support	Load	Gas permeability (barrers)		Selectivity	Ref.
		CO	N_2	CO/N_2	
PES	$[TEA][CuCl_2]$	170.5	6.8	25.1	This work[a]
Hydrophilic PVDF	CuCl/[hmim][Cl] (0.38:1)	20.6	7.6	2.7	[9][a]
Hydrophilic PVDF	CuCl/[hmim][Cl] (0.5:1)	37.3	11.4	2.8	[9][b]
Hydrophobic PP	CuCl/[hmim][Cl] (2:1)	~3.9	~1.5	~2.5	[10][b]
Matrimid® 5218	-	0.44	0.19	2.44	[11][c]
Matrimid® dense film	-	0.40	0.27	2.02	[12][d]

[a] Operating condition: 1.5 bar, 40 ºC.

[b] Operating condition: 1.5 bar, 50 ºC.

[c] Operating condition: 30 ºC.

[d] Operating condition: 2 bar, 30 ºC.

10. Theoretical calculations. All the geometries were fully optimized with Gaussian 09 program using B3LYP method based on density functional theory [S1]. LANL2DZ basis set was used for Cu and 6-311+G* basis set for other atoms. The calculation was performed in condensed phase with the Polarizable Continuum Model (PCM). This method creates the solute cavity via a set of overlapping spheres. The dielectric constant of the solvent was set as 15.2 to simulate the environment of ionic liquid. All of the structures were fully optimized with above methods. Energy calculations as well as Zero-point energy (ZPE) correction have been done by using the same level of theory. The computed stationary points have been characterized as minima by diagonalizing the Hessian matrix and analyzing the vibrational normal modes. In this way, the stationary points can be classified as minima if no imaginary frequencies are shown.

Reference:

[S1] M. J. Frisch, G. W. Trucks, H. B. Schlegel, G. E. Scuseria, M. A. Robb, J. R. Cheeseman, J. A. Montgomery, Jr., T. Vreven, K. N. Kudin, J. C. Burant, J. M. Millam, S. S. Iyengar, J. T omasi, V. Barone, B. Mennucci, M. Cossi, G. Scalmani, N. Rega, G. A. Petersson, H. Nakatsu ji, M. Hada, M. Ehara, K. Toyota, R. Fukuda, J. Hasegawa, M. Ishida, T. Nakajima, Y. Honda, O. Kitao, H. Nakai, M. Klene, X. Li, J. E. Knox, H. P. Hratchian, J. B. Cross, V. Bakken, C. Adamo, J. Jaramillo, R. Gomperts, R. E. Stratmann, O. Yazyev, A. J. Austin, R. Cammi, C. P omelli, J. Ochterski, P. Y. Ayala, K. Morokuma, G. A. Voth, P. Salvador, J. J. Dannenberg, V. G. Zakrzewski, S. Dapprich, A. D. Daniels, M. C. Strain, O. Farkas, D. K. Malick, A. D. Rab uck, K. Raghavachari, J. B. Foresman, J. V. Ortiz, Q. Cui, A. G. Baboul, S. Clifford, J. Cioslo wski, B. B. Stefanov, G. Liu, A. Liashenko, P. Piskorz, I. Komaromi, R. L. Martin, D. J. Fox, T. Keith,M. A. Al-Laham, C. Y. Peng, A. Nanayakkara, M. Challacombe, P. M. W. Gill, B. G. Johnson, W. Chen, M. W. Wong, C. Gonzalez, J. A. Pople, GAUSSIAN 09, Gaussion, Inc., Pittsburgh, PA, 2009.

11. Equilibrium thermodynamic properties of CO absorption in PCILs. An equilibrium model which can explain quantitatively the occurring reactions and phenomena is discussed to describe the process in the gas-liquid absorption. According to our group's previous work on SO_2 absorption,[13] there are also two aspects of absorption in PCIL-CO systems: physical and chemical. Firstly we supposed that all the copper (I) introduced in the reaction medium was active for the σ-π complexation reaction, one PCIL molecule could chemically attract one CO molecule, and the complexation strengths of CO with different copper based anion species were equal. In addition, owing to the fact that the binding site is only on the anion of PCIL,

the absorption process (both physical and chemical) can be simplified into the two equilibrium reactions as shown in Eqs. (S3) and (S4):

$$CO\ (g) \leftrightharpoons CO\ (l) \tag{S3}$$

$$CO\ (l) + CuCl_n^{(n-1)-}(l) \leftrightharpoons Cu(CO)Cl_n^{(n-1)-}(l) \tag{S4}$$

The overall reaction can be expressed into the following equation:

$$CO\ (g) + IL\ (l) \leftrightharpoons CO\text{-}IL\ (l) \tag{S5}$$

The Henry's law for the physical absorption of CO in liquid phase is defined in terms of molality and expressed into Eq (S6). P is the partial pressure of CO in kPa, H is the Henry's law constant in kPa, and m_{CO} is the concentration of physically dissolved CO in mol·kg^{-1}. The chemical reaction equilibrium of Eq. (S4) is expressed into Eq. (S7), where Ko 1 is the equilibrium constant, γ_{CO}, γ_{IL} and γ_{COIL} are the activity coefficients of the physically dissolved CO, free IL and CO-IL complex in the liquid phase, respectively. m_{IL} and m_{COIL} are the concentrations of the IL and the CO-IL complex in mol·kg^{-1} and m^o is the standard molality (1 mol·kg^{-1}). Similarly, the overall reaction equilibrium corresponding to Eq. (S5) is formulated using Eq. (S8), where K^o is the equilibrium constant of the overall reaction and P^o is the standard pressure (100kPa). Eq. (S9) is the mass balance of the IL, where m_{IL_0} is the initial concentration of the IL and is a constant that can be calculated from Eq. (S11). M_{IL} is the molar mass of the IL in g·mol^{-1}. The mass balance of CO is given in Eq. (S10), where m_t is the total concentration of CO in the liquid phase.

$$P = H\gamma_{CO}\frac{m_{CO}}{m^o} \tag{S6}$$

$$Ko\ 1 = \frac{\gamma_{COIL}\dfrac{m_{COIL}}{m^o}}{\gamma_{CO}\dfrac{m_{CO}}{m^o}\cdot\gamma_{IL}\dfrac{m_{IL}}{m^o}} \tag{S7}$$

$$K^{o} = \frac{\gamma_{COIL}\dfrac{m_{COIL}}{m^{o}}}{\dfrac{P}{P^{o}}\cdot\gamma_{IL}\dfrac{m_{IL}}{m^{o}}} \tag{S8}$$

$$m_{IL_0} = m_{IL} + m_{COIL} \tag{S9}$$

$$m_t = m_{CO} + m_{COIL} \tag{S10}$$

$$m_{IL_0} = \frac{1}{M_{IL}}\cdot 10^{3} \tag{S11}$$

It is not easy to calculate the activity coefficients of the three species in the liquid phase of the reaction system. However, ideal diluted solution can be easily fulfilled and all the activity coefficients tend to be unity when the concentration of free CO in the liquid is low. In fact, only the products of activity coefficients are required in the calculation of Ko 1 and K^{o} as shown in Equations. (S7) and (S8). Therefore, it is reasonable to assume that the products of activity coefficients in Equations. (S7) and (S8) are constant during the whole absorption process to avoid the calculation of activity coefficient. After simple deduction, the following equation is obtained to relate the total solubility of CO in ILs to the partial pressure of CO.

$$m_t = \left(\frac{m_{IL_0}}{P + \dfrac{H}{K_1^{o}}} + \frac{1}{H}\right)P \tag{S12}$$

Combining Eqs. (S6), (S7) and (S8) results in Eq. (S13):

$$K^{o} = \frac{K_1^{o}}{H}P^{o} \tag{S13}$$

The correlation of experimental solubility of CO in PCILs using Eq. (S12) (correlation coefficient R^2>0.99) results in the values of Henry's law constant and the reaction equilibrium constant of Eq. (S4). The reaction equilibrium constant of Eq. (S5) can be obtained from Eq. (S13). All the calculated values of H and K^{o} are summarized in Table S5. The molar reaction

enthalpy of Eq. (S5), ΔH (the heat of absorption process), is calculated using the van't Hoff equation (see Eq. (S14)) by drawing a linear fit of ln K^o with 1/T. ΔH data are also shown in Table S5.

$$\frac{dlnK^o}{d(1/T)} = -\frac{\Delta H}{R} \quad \text{(S14)}$$

Table S5 Equilibrium thermodynamic properties of CO in PCILs in the process of gas-liquid absorption.

PCILs	T(K)	H(kPa)	$K^o \times 10^3$	ΔH (kJ/mol)
[TEA][$CuCl_2$]	303.15	2166.4	70.63	-29.1 (R^2=0.9992)
	313.15	9069.6	49.59	
	328.15	18116.9	29.22	
[TPA][$CuCl_2$]	303.15	1806.1	90.40	-47.8 (R^2=0.9955)
	313.15	2503.7	51.77	
	323.15	3581.3	27.93	

References:

1. A. Du, B. Zhou, W. W. Xu, Q. J. Yu, Y. Shen, Z. H. Zhang, J. Shen and G. M. Wu, *Langmuir*, 2013, **29**, 11208-11216
2. J. Zhang, J. S. Xu, H, Zhang, X. Y. Yin, J. H. Qian, L. L. Liu, D. J. Yang and X. Y. Liu, *Micro & Nano Letters*, 2011, **6**, 119-121
3. K. Huang, X. M. Zhang, Y. X. Li, Y. T. Wu and X. B. Hu, *J. Membr. Sci.*, 2014, **471**, 227-236.
4. K. Huang, X. Zhang, X. B. Hu and Y. T. Wu, *AIChE J.*,2016, **62**, 4480-4490.

5. Zhang, X. M., Tu, Z. H., Li, H. *et al.* Selective separation of H_2S and CO_2 from CH_4 by supported ionic liquid membranes. *J. Membr Sci*. **543** 282-287 (2017).
6. X. M. Zhang, Z. H. Tu, H. Li, K. Huang, X. B. Hu, Y. T. Wu and D. R. MacFarlane, *J. Membr. Sci*., 2017, **543**, 282-287.
7. K. Huang, X. M. Zhang, Y. X. Li, Y. T. Wu and X. B. Hu, *J. Membr. Sci*., 2014, **471**, 227-236.
8. Y. Y. Jiang, Z. Zhou, Z. Jiao, L. Li, Z. B. Zhang and Y. T. Wu, *J. Phys. Chem. B,* 2007, **111**, 5058-5061.
9. G. Zarca, I. Ortiz, A. Urtiaga, *J. Membr. Sci.,* 2013, **438**, 38-45.
10. G. Zarca, I. Ortiz and A. Urtiaga, *Chem. Eng. Res. Des*., 2014, **92**, 764-768.
11. C. David, D. Gorri, A. Urtiaga and I. Ortiz, *J. Membr. Sci*., 2011, **378**, 359-368.
12. David, D. Gorri, K. Nijmeijer, I. Ortiz and A. Urtiaga, *J. Membr. Sci*., 2012, **419-420**, 49-56.
13. K. Huang, Y. L. Chen, X. M. Zhang, S. Xia, Y. T. Wu and X. B. Hu, *Chem. Eng. J.,* 2014, **237**, 478-486.